Update on coupled dark energy and the H_0 tension

Adrià Gómez-Valent, Valeria Pettorino, Luca Amendola

Update on coupled dark energy and the H_0 tension

Adrià Gómez-Valent,[1,*] Valeria Pettorino,[2,†] and Luca Amendola[1,‡]
[1]*Institut für Theoretische Physik, Ruprecht-Karls-Universität Heidelberg, Philosophenweg 16, D-69120 Heidelberg, Germany*
[2]*AIM, CEA, CNRS, Université Paris-Saclay, Université Paris Diderot, Sorbonne Paris Cité, F-91191 Gif-sur-Yvette, France*

(Received 10 April 2020; accepted 21 May 2020; published 15 June 2020)

In this work, we provide updated constraints on coupled dark energy (CDE) cosmology with Peebles-Ratra (PR) potential and constant coupling strength β. This modified gravity scenario introduces a fifth force between dark matter particles, mediated by a scalar field that plays the role of dark energy. The mass of the dark matter particles does not remain constant, but changes with time as a function of the scalar field. Here we focus on the phenomenological behavior of the model, and assess its ability to describe updated cosmological datasets that include the *Planck* 2018 cosmic microwave background (CMB) temperature, polarization and lensing, baryon acoustic oscillations, the Pantheon compilation of supernovae of Type Ia, data on $H(z)$ from cosmic chronometers, and redshift-space distortions. We also study the impact of the local measurement of H_0 from SH0ES and the strong-lensing time delay data from the H0LICOW Collaboration on the parameter that controls the strength of the interaction in the dark sector. We find a peak corresponding to a coupling $\beta > 0$ and to a potential parameter $\alpha > 0$, more or less evident depending on the dataset combination. We show separately the impact of each dataset and remark that CMB lensing is especially the one dataset that shifts the peak the most towards ΛCDM. When a model selection criterion based on the full Bayesian evidence is applied, however, ΛCDM is still preferred in all cases, due to the additional parameters introduced in the CDE model.

DOI: 10.1103/PhysRevD.101.123513

I. INTRODUCTION

Important observational hints in favor of the positive acceleration of the Universe appeared already more than twenty years ago, thanks to the detection of standardizable high-redshift supernovae of Type Ia (SNIa) and the measurement of their light curves and redshifts [1,2]. Since then, many other probes have contributed to increase the evidence in favor of the late-time accelerated phase. They range, e.g., from the detection of the baryon acoustic peak in the two-point correlation function of matter density fluctuations [3,4] to the very accurate measurement of the cosmic microwave background (CMB) temperature anisotropies by WMAP [5] and *Planck* [6–8]. At the phenomenological level, the easiest explanation for such acceleration is given by the presence of a very tiny cosmological constant in Einstein's field equations, with an associated energy density which is orders of magnitude lower than the quantum field theoretical estimates made for the vacuum energy density. Protecting such a low value from radiative corrections is extremely difficult and constitutes the core of the so-called "old" cosmological constant problem, cf. e.g., Refs. [9–11]. In addition, explaining why the current value of this energy density is of the same order of magnitude as the matter energy density, the so-called "coincidence problem" is considered by part of the cosmological community as another problem that needs to be addressed. The cosmological constant is a pivotal ingredient of the standard cosmological model, also known as ΛCDM or the concordance model (cf. e.g., the reviews in Refs. [12,13]), which can explain most of the cosmological observations with high proficiency. Nevertheless, the aforementioned theoretical conundrums, together with a few persistent tensions in some relevant parameters of the model as the Hubble parameter H_0 [8,14] and the root-mean-square of mass fluctuations at scales of $8h^{-1}$ Mpc [15], σ_8 [or $S_8 = \sigma_8(\Omega_m^{(0)}/0.3)^{0.5}$ [16]],[1] with h being the reduced Hubble parameter, motivate theoretical cosmologists to look for alternative scenarios in which these problems can be solved, or at least alleviated; see Refs. [17,18] and references therein. Wherever the solution comes from—i.e., a departure from general relativity or some sort of new field describing dark energy (DE)—it must mimic very well the behavior of a cosmological

*gomez-valent@thphys.uni-heidelberg.de
†valeria.pettorino@cea.fr
‡l.amendola@thphys.uni-heidelberg.de

[1]The superscripts (0) will denote from now on quantities evaluated at present, i.e., at $a = 1$.

constant at low redshifts, meaning that the corresponding effective equation of state (EOS) parameter must be very close to -1, and that the new component must not be able to cluster efficiently at low scales.

In this paper, we consider a scenario in which dark matter (DM) particles interact via a force mediated by a scalar field, which in turn drives cosmic acceleration. This scenario is referred to as *coupled dark energy* (CDE). It was originally proposed as a means of alleviating the coincidence problem [19,20], considering not only a potential energy density for quintessence to generate its dynamics, but also allowing an interaction with other sectors of the theory. These interactions extended the original quintessence models [21–24]. They cannot be ruled out *a priori*, and hence, they must be duly constrained by experiments and observations.

Some works already set constraints on this model, but using older cosmological datasets—for instance, CMB data from the WMAP satellite and the South Pole Telescope [25], or considering past (2013, 2015) releases of *Planck* CMB data in combination with other datasets, as, e.g., from baryon acoustic oscillations (BAO) and SNIa [26,27]. Intriguingly, these works detected a likelihood peak at a nonvanishing value of the coupling constant. One of the main goals of this paper is then to critically revisit and update these results in the light of the recent strengthening of the H_0 tension and of the rich amount of currently available data at our disposal, in particular the *Planck* 2018 CMB temperature, polarization, and lensing data, but also other new cosmological data—for instance, Refs. [28,29]. For constraints on other models with DM-DE interactions, see, e.g., Refs. [30–43], and when the interaction is motivated in the context of the running vacuum models [39,40,44–46].

II. COUPLED DARK ENERGY

We consider a CDE scenario, as studied in Refs. [20,47,48], to which we refer for a detailed description. We here briefly recall the main equations. This CDE model is formulated in the so-called Einstein or observational frame [49]. Apart from the standard model of particle physics and a potential extension accounting for the origin of the neutrino masses, we consider a dark sector described by the following Lagrangian density:

$$\mathcal{L}_{\rm dark} = -\partial_\mu\phi\partial^\mu\phi - V(\phi) - m(\phi)\bar{\psi}\psi + \mathcal{L}_{\rm kin}[\psi], \quad (1)$$

where ϕ is the scalar field that plays the role of DE, with potential $V(\phi)$, and ψ is the DM field, considered here to be of fermionic nature, just for illustrative purposes. The DM particles interact with the DE due to the ϕ-dependent mass term appearing in Eq. (1). Such interaction introduces a fifth force that alters the trajectory in space-time of the DM with respect to the one found in the uncoupled case. Depending on the strength of the force, this model can be force-accelerated, as opposed to fluid-accelerated, adopting the terminology of Ref. [49]. As we do not couple ϕ to the standard model sector, we avoid the stringent local (Solar System) constraints on the violation of the weak equivalence principle [50], and also on screened fifth forces that couple ϕ to nondark matter, e.g., from Casimir experiments [51], precision measurements of the electron magnetic moment [52], or measurements of the Eötvös parameter [53]. They have no impact on the CDE model under study.

The variation of the total action with respect to the metric leads as usual to Einstein's equations, and the covariant energy of the joint system DM-DE is conserved. Hence, $\nabla^\mu T^\phi_{\mu\nu} = +Q_\nu$ and $\nabla^\mu T^{dm}_{\mu\nu} = -Q_\nu$, with Q_ν defined as

$$Q_\nu = \beta\kappa T^{dm}\nabla_\nu\phi, \quad (2)$$

where $\kappa = \sqrt{8\pi G}$, T^{dm} is the trace of the DM energy-momentum tensor, and β controls the strength of the interaction and is in general a function of ϕ. If it is set to zero, we recover the equations of uncoupled quintessence. In this work, we consider β to be a positive constant.

We assume that the Universe is spatially flat, as supported by CMB information from *Planck* 2018 when combined with BAO [8] and/or SNIa [54], with the curvature parameter $\Omega_K^{(0)}$ constrained to be lower than $\sim$2% at 68% C.L. in ΛCDM. Thus, we can make use of the Friedmann-Lemaître-Robertson-Walker metric, which at the background level reads $ds^2 = a^2(\tau)[-d\tau^2 + \delta_{ij}dx^i dx^j]$, with a being the scale factor, τ the conformal time, and x^i for $i = 1, 2, 3$ the spatial comoving coordinates. In addition, we treat DM as a pressureless perfect fluid, so the conservation equations for DE and DM can be written, respectively,

$$\beta\kappa a^2\rho_{dm} = \phi'' + 2\mathcal{H}\phi' + a^2\frac{\partial V}{\partial\phi}, \quad (3)$$

$$\rho'_{dm} + 3\mathcal{H}\rho_{dm} = -\beta\kappa\rho_{dm}\phi', \quad (4)$$

with ρ_{dm} being the DM energy density, $\mathcal{H} = a'/a$, and the primes denoting derivatives with respect to the conformal time. All the functions entering these equations are background quantities. If we assume the conservation of the number density of DM particles, then their mass evolves as $m(\phi) = m^{(0)}e^{\beta\kappa(\phi^{(0)}-\phi)}$.

A feature of the model is that for $\beta^2 < 3/2$, it has an unstable (saddle) fixed point at $(\Omega_{dm}, \Omega_\phi) = (1 - 2\beta^2/3, 2\beta^2/3)$, where $\Omega_i = \rho_i/\rho_c$, with ρ_c being the critical energy density. This fixed point (dubbed ϕMDE in Ref. [20]) cannot be reached exactly, since there is also a non-null fraction of baryons, but the system can be quite close to it, since the DM energy density is much larger than the baryonic one (cf. Fig. 1). During this phase, the effective EOS parameter—i.e., the ratio of the total pressure and the

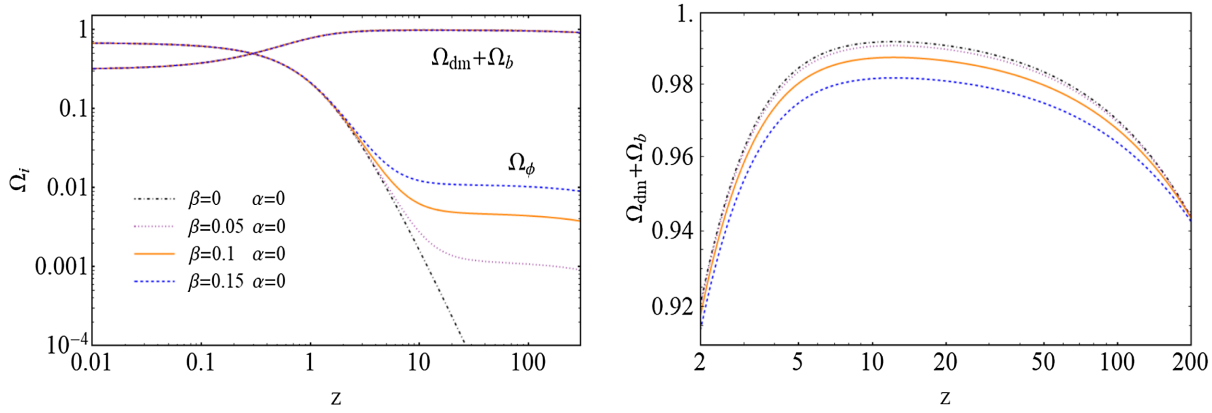

FIG. 1. *Left:* Normalized densities $\Omega_{dm}(z)+\Omega_b(z)$ and $\Omega_\phi(z)$ for four alternative values of β and considering a constant potential. The other parameters (including the current energy densities) have been set to the best-fit ΛCDM values from the TTTEEE + lowE *Planck* 2018 analysis [8]. *Right:* Here we zoom in the range $z=[2,200]$ of the $\Omega_{dm}+\Omega_b$ curves in order to better visualize their evolution during the matter-dominated epoch, when the system is near the ϕMDE fixed point. See the text for details.

critical energy density in the Universe, is given by $w_{\rm eff}=\Omega_\phi$, and hence the deceleration parameter reads $q=\frac{1}{2}(1+3w_{\rm eff})=\frac{1}{2}+\beta^2$. Thus, the coupling between DM and DE makes the Universe more decelerated with respect to the uncoupled quintessence case during the matter-dominated epoch (MDE). This fact, together with the fifth force that enters now as a new source term in the Poisson equation, helps matter inhomogeneities to grow faster for larger values of β. We also remark that for fixed values of the present energy densities, matter becomes dominant over radiation earlier in time when $\beta>0$, with respect to the uncoupled case. In the CDE scenario, the equation for the DM density contrast $\delta_{dm}=\delta\rho_{dm}/\rho_{dm}$, at deep subhorizon scales ($k\gg\mathcal{H}$) and when nonlinear processes are unimportant, reads

$$\delta''_{dm}+(\mathcal{H}-\beta\kappa\phi')\delta'_{dm} - 4\pi G a^2[\rho_b\delta_b+\rho_{dm}\delta_{dm}(1+2\beta^2)]=0. \quad (5)$$

If we neglect the contribution of baryons, $\delta_m(a)\sim a^{1+2\beta^2}$. Hence, larger values of β enhance the matter power spectrum (see the left plot of Fig. 2) and leave an imprint on the CMB temperature anisotropies. First, the integrated Sachs-Wolfe effect [55] is enhanced during the MDE earlier than in the uncoupled scenario, in which such effect is only relevant after matter-domination; second, the coupling affects the lensing of CMB by large-scale structure; the interaction also shifts the position of the acoustic peaks to larger multipoles due to the decrease of the sound horizon at the baryon-drag epoch, which is caused by the increase of the mass of the DM particles (this latter effect is, however, typically very small and subdominant). Finally, the amplitude is suppressed, because of the decrease of ρ_b/ρ_{dm} at recombination. These two effects explain why the coupling strength is degenerate with the Hubble parameter today [26], whose value is related to the position and overall amplitude of the first peak. These and other aspects of the structure formation were already discussed in

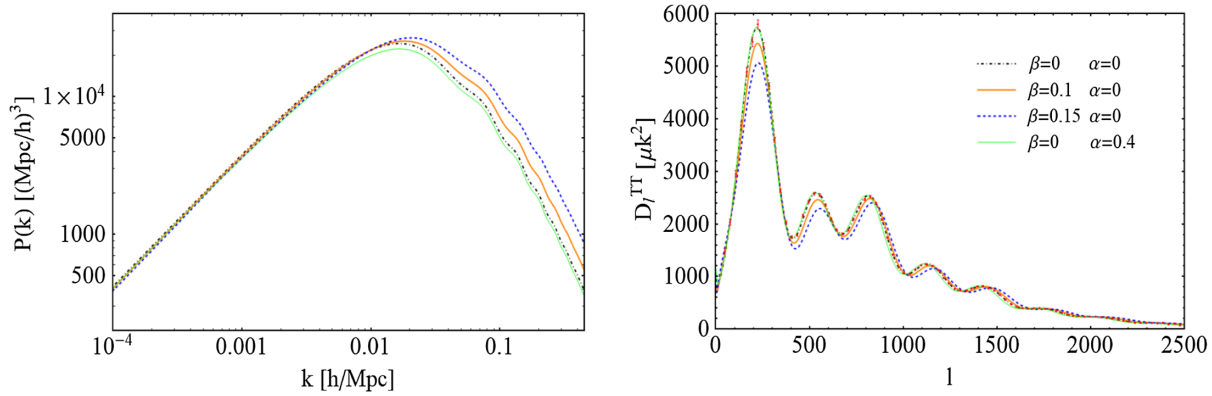

FIG. 2. Theoretical curves of the current matter power spectrum (left plot) and CMB temperature anisotropies (right plot) for the ΛCDM, two CDE models with $\beta=0.1$, 0.15 and flat potential, and also for the uncoupled Peebles-Ratra model with $\alpha=0.4$. We set the other parameters as in Fig. 1. In the right plot, we also include the observational data from Ref. [8] (in red). These figures show (i) the enhancement of the growth of matter perturbations caused by $\beta>0$, and the opposite effect produced by $\alpha>0$; and (ii) the shift to larger multipoles and the amplitude suppression of the acoustic peaks induced by increasing values of β. See the text for further details.

TABLE I. Constraints obtained using the dataset combinations described in Sec. IV B on the following parameters of the CDE model: the reduced DM and baryon energy densities, $\Omega_{dm}^{(0)}h^2$ and $\Omega_b^{(0)}h^2$; the reionization optical depth, τ; the Hubble parameter, H_0 (in units of km/s/Mpc); the power of the primordial power spectrum, n_s; the current amplitude of mass fluctuations at $8h^{-1}$ Mpc, σ_8; the coupling strength β; and the power of the PR potential [Eq. (6)]. We remark that these are not the primary parameters that are varied in the Monte Carlo analyses (cf. Appendix A for details). We provide the mean values and 68% confidence intervals for each of them. In the last two rows, we show the differences with respect to the ΛCDM of the minimum values of the χ^2 function, and also the natural logarithm of the Bayes ratio $B_{\mathrm{CDE},\Lambda}$, as defined in Eqs. (11) and (12). The (small) negative values of $\chi^2_{\mathrm{min,CDE}} - \chi^2_{\mathrm{min},\Lambda}$ tell us that CDE is able to fit slightly better the data than the ΛCDM; if we use as an alternative estimator the Bayes factor, we find negative values of $\ln(B_{\mathrm{CDE},\Lambda})$, indicating a preference for the ΛCDM model. See Sec. V for a thorough discussion of the results.

Parameter	P18	P18 + BSC	P18 + SH0ES+ H0LICOW	P18 + BSC + RSD	P18lens + BSC + RSD	P18 + BSC + SH0ES+ H0LICOW	P18lens + SH0ES+ H0LICOW
$\Omega_{dm}^{(0)}h^2$	$0.1207^{+0.0014}_{-0.0013}$	0.1192 ± 0.0008	$0.1172^{+0.0012}_{-0.0014}$	0.1187 ± 0.0008	0.1191 ± 0.0007	0.1185 ± 0.0008	$0.1182^{+0.0011}_{-0.0010}$
$\Omega_b^{(0)}h^2$	0.02237 ± 0.00015	$0.02242^{+0.00010}_{-0.00015}$	$0.02262^{+0.00016}_{-0.00014}$	$0.02253^{+0.00010}_{-0.00012}$	$0.02253^{+0.00013}_{-0.00011}$	$0.02253^{+0.00011}_{-0.00013}$	$0.02259^{+0.00014}_{-0.00016}$
τ	0.0538 ± 0.0070	$0.0532^{+0.0075}_{-0.0087}$	0.0594 ± 0.0074	0.0501 ± 0.0052	$0.0525^{+0.0052}_{-0.0064}$	$0.0579^{+0.0069}_{-0.0078}$	$0.0637^{+0.0065}_{-0.0096}$
H_0	$67.74^{+0.57}_{-0.66}$	68.41 ± 0.38	$69.43^{+0.72}_{-0.53}$	$68.64^{+0.30}_{-0.38}$	68.45 ± 0.34	$68.79^{+0.35}_{-0.40}$	68.99 ± 0.51
n_s	$0.9654^{+0.0035}_{-0.0042}$	0.9690 ± 0.0038	0.9731 ± 0.0042	$0.9701^{+0.0029}_{-0.0033}$	0.9685 ± 0.0034	0.9705 ± 0.0034	0.9713 ± 0.0037
σ_8	0.8164 ± 0.0076	0.8104 ± 0.0076	$0.8121^{+0.0065}_{-0.0080}$	0.8048 ± 0.0052	$0.8073^{+0.0048}_{-0.0056}$	0.8120 ± 0.0074	0.8160 ± 0.0068
α	<0.50	0.52 ± 0.17	1.32 ± 0.18	$0.67^{+0.11}_{-0.16}$	$0.25^{+0.09}_{-0.20}$	$0.73^{+0.11}_{-0.27}$	$0.33^{+0.19}_{-0.23}$
β	$0.0158^{+0.0067}_{-0.0120}$	$0.0206^{+0.0070}_{-0.0095}$	$0.0294^{+0.0120}_{-0.0076}$	$0.0151^{+0.0073}_{-0.0083}$	$0.0095^{+0.0030}_{-0.0087}$	$0.0206^{+0.0076}_{-0.0100}$	$0.0197^{+0.0094}_{-0.0084}$
$\chi^2_{\mathrm{min,CDE}} - \chi^2_{\mathrm{min},\Lambda}$	−0.02	−0.28	−0.58	−1.56	−0.90	−1.34	−1.46
$\ln B_{\mathrm{CDE},\Lambda}$	−8.05	−9.95	−7.57	−8.33	−7.83	−7.95	−8.75

Refs. [48,56–58]. See therein for further details, and also the plots in Fig. 2.

The quintessence potential only rules the dynamics of ϕ in the late-time universe, after the MDE, when the interaction term appearing on the lhs of Eq. (3) becomes subdominant. It helps to slow down structure formation processes with respect to the flat-potential scenario (for a fixed value of the current DE density). Hence, it can compensate in lesser or greater extent (depending on its steepness) the enhancement of power generated by the fifth force during the MDE (cf. the left plot of Fig. 2 and its caption).

We employ the Peebles-Ratra (PR) potential [23,24],

$$V(\phi) = V_0\phi^{-\alpha}, \tag{6}$$

with V_0 and $\alpha > 0$ being constants, and the former having dimensions of mass$^{4+\alpha}$ in natural units, since ϕ has dimensions of mass. We want to update the constraints on the parameters of the CDE model with PR potential that were obtained in some past works using older CMB data, from WMAP and/or past releases of *Planck* (cf. Refs. [25–27,59]), so it is natural to stick to Eq. (6) here. Another reason is that it has proved to be capable of improving the description of some cosmological datasets with respect to the ΛCDM model in the noninteractive case [60–62].

The CDE model we are considering (i.e., CDE with PR potential) has three nested models—namely the ΛCDM, the PR model, and the CDE model with flat potential. They are obtained from the full CDE model with Eq. (6) in the limits $(\alpha, \beta) \to (0, 0)$, $\beta \to 0$, and $\alpha \to 0$, respectively. We also provide constraints on these scenarios in Appendix B.

For recent studies on CDE with an exponential potential, see Refs. [30,32,33,42]. We report fitting results for this model too, in Appendix C.

III. METHODOLOGY

We have implemented the CDE model described in Sec. II in our own modified version of the Einstein-Boltzmann system solver CLASS[2] [63], which allows us to solve the background and linear perturbations equations and produce the theoretical quantities of interest, as, e.g., the matter power spectrum, the CMB anisotropies, the cosmological distances, etc. This implementation has been compared and validated with the interacting dark energy anisotropy (IDEA) code, used in Refs. [25,27,64,65]. The Bayesian exploration of the parameter space of the model in the light of the various datasets described in Sec. IV has been carried out with the Monte Carlo sampler MontePython[3] [66]. Our code lets us skip the shooting method that is employed in IDEA to match the initial conditions with the current values of the cosmological energy densities, and this allows us to improve the computational efficiency of our Markov chain Monte Carlo (MCMC) analyses, cf. Appendix A for details. We have also used the PYTHON package GetDist[4] [67] to process the chains and obtain the mean values and uncertainties of the parameters reported in Tables I–III, as well as the contours of Figs. 3 and 4. Finally, we have computed the full

[2]http://lesgourg.github.io/class_public/class.html.
[3]http://baudren.github.io/montepython.html.
[4]https://getdist.readthedocs.io/en/latest/.

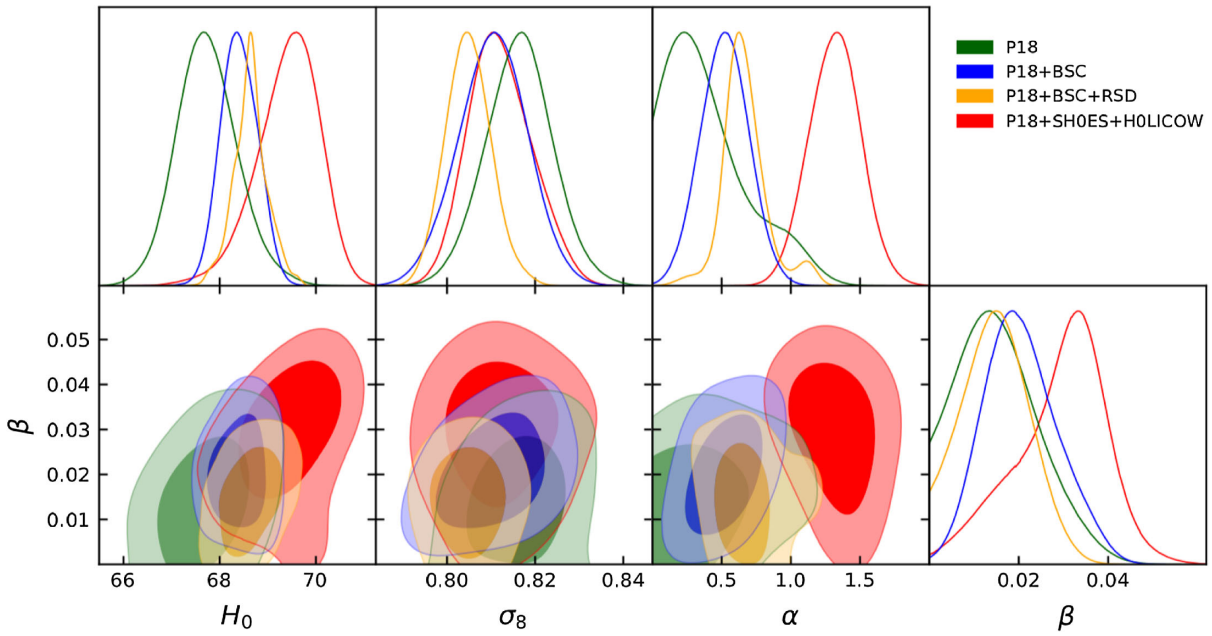

FIG. 3. 1σ and 2σ confidence contours obtained using some of the combined datasets described in Sec. IV B in the (H_0, β), (σ_8, β), and (α, β) planes, together with the marginalized one-dimensional posterior distributions for these parameters. See the discussion of these results in Sec. V.

Bayesian evidences for all the models and under the various datasets, by processing the corresponding Markov chains with the code MCEvidence[5] [68]. This has allowed us to carry out a rigorous model comparison analysis, which we present in Sec. V.

IV. DATA

Since the last fitting analysis of the CDE model with PR potential, in Ref. [27], new and more precise data have appeared in the literature. In this paper, we perform an exhaustive update of the datasets with respect to those used in Ref. [27]. The most important changes are that (i) here we make use of the *Planck* 2018 CMB data [8] instead of the 2015 release [7]; (ii) we fully update our BAO and redshift-space distortion (RSD) datasets, using now, e.g., the data of the last release of the Baryon Oscillation Spectroscopic Survey[6] (BOSS); (iii) we substitute the SNIa sample from the Joint-Light-curve Analysis (JLA) [69] by the Pantheon + MCT compilation [70,71], which contains the former and includes 323 additional SNIa; (iv) we study the impact of the data on $H(z)$ obtained from cosmic chronometers (CCH); (v) instead of using the prior on H_0 from Ref. [72], $H_0 = (70.6 \pm 3.3)$ km/s/Mpc, we use the measurement by the SH0ES Collaboration reported in Ref. [14] (see Sec. IV A 6 and comments therein); and (vi) we also study the effect that the inclusion of the strong-lensing time delay distances measured by H0LICOW has on our constraints. We use, therefore, a much richer dataset here than the one employed in Ref. [27].

Our dataset is very similar to the one used by the *Planck* Collaboration in their 2018 analysis of the ΛCDM and minimal extensions of it [8]. There are some differences, though—e.g., we analyze here the effect of cosmic chronometers and the H0LICOW data, something that was not done there. We refer the reader to Sec. IV A and Ref. [8] for details.

A. Description of the individual datasets

Here we list and describe the individual datasets that we employ in this work to constrain the CDE model that we have presented in Sec. II, and its nested models. We will study their impact by considering different dataset combinations, as explained in Sec. IV B.

1. Cosmic microwave background

We derive all the main results of this paper, making use of the full TTTEEE + lowE CMB likelihood from *Planck* 2018 [8], which includes the data on the CMB temperature (TT) and polarization (EE) anisotropies, and their cross-correlations (TE) at both low and high multipoles. We also study what is the impact of also including the CMB lensing likelihood [73]. Temperature and polarization spectra are already lensed; however, the CMB lensing likelihood includes on top of lensed spectra also the four-point correlation function. Lensing peak sensitivity is to lenses at $z \approx 2$, halfway to the last scattering surface, with deflection effects at redshifts which are relevant for dark energy models such as CDE. It has in particular been

[5]https://github.com/yabebalFantaye/MCEvidence.
[6]http://www.sdss3.org/surveys/boss.php.

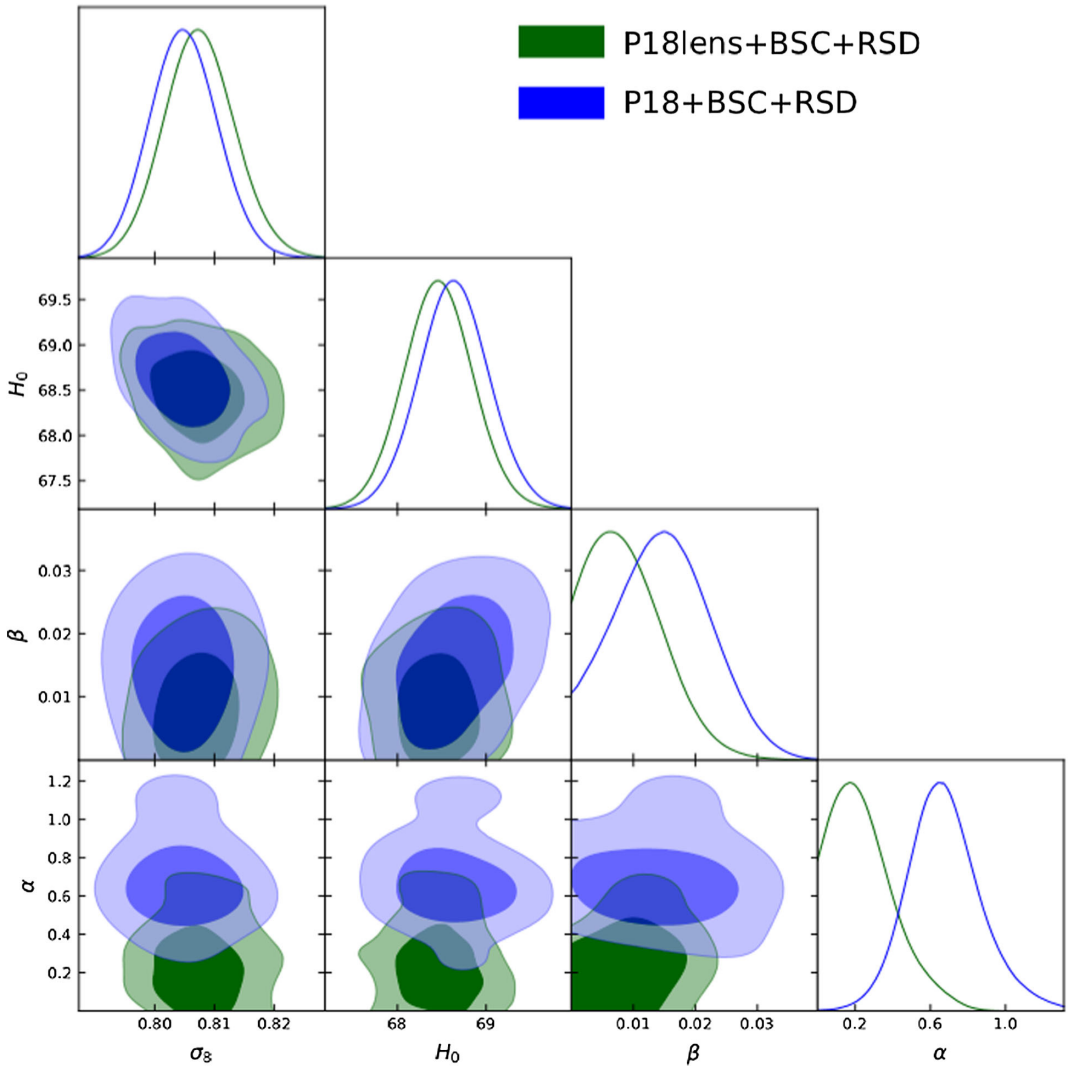

FIG. 4. 1σ and 2σ confidence contours obtained with the P18 + BSC + RSD and P18lens + BSC + RSD datasets in the most relevant two-dimensional planes of the CDE model parameter space. They allow us to see what is the impact of the CMB lensing on our results. We also show the corresponding marginalized one-dimensional posterior distributions for all the parameters. See the related comments in Sec. V.

shown in Ref. [27] that CMB lensing pushes constraints towards ΛCDM. As stated in Ref. [8], we note that the lensing likelihood assumes a fiducial ΛCDM model, with linear corrections to the fiducial model accounted for self-consistently. According to Ref. [8], this procedure is unbiased, at least up to when the lensing spectrum differs from the fiducial spectrum by as much as 20%, estimated to be larger than the differences allowed by the CMB lensing data. While further independent validation of such tests would be interesting for future analyses on modified gravity, we find it important to comment on results with/without CMB lensing inclusion for the purpose of testing nonminimal extensions of ΛCDM, such as CDE.

2. Baryon acoustic oscillations

Baryon acoustic oscillations are a direct consequence of the strong coupling between photons and baryons in the pre-recombination epoch. After the decoupling of photons, the overdensities in the baryon fluid evolved and attracted more matter, leaving an imprint in the two-point correlation function of matter fluctuations with a characteristic scale of around 147 Mpc that can be used as a standard ruler and to constrain cosmological models. It was first measured by Refs. [3,4] using the galaxy power spectrum. Since then, several galaxy surveys have been able to provide precise data on BAO, either in terms of the dilation scale D_V,

$$\frac{D_V(z)}{r_d} = \frac{1}{r_d}\left[D_M^2(z)\frac{cz}{H(z)}\right]^{1/3}, \tag{7}$$

with $D_M = (1+z)D_A(z)$ being the comoving angular diameter distance and r_d the sound horizon at the baryon drag epoch, or even by splitting (when possible) the transverse and line-of-sight BAO information and hence

being able to provide data on $D_A(z)/r_d$ and $H(z)r_d$ separately, with some degree of correlation. The surveys provide the values of the measurements at some effective redshift(s). We employ the following BAO data points:

(1) D_V/r_d at $z = 0.122$ provided in Ref. [74], which combines the dilation scales previously reported by the 6dF Galaxy Survey[7] (6dFGS) [75] at $z = 0.106$ and the one obtained from the Sloan Digital Sky Survey[8] (SDSS) Main Galaxy Sample at $z = 0.15$ [76].
(2) The anisotropic BAO data measured by BOSS using the LOWZ ($z = 0.32$) and CMASS ($z = 0.57$) galaxy samples [77].
(3) The dilation scale measurements by WiggleZ[9] at $z = 0.44, 0.60, 0.73$ [78]. The galaxies contained in the WiggleZ catalog are located in a patch of the sky that partially overlaps with those present in the CMASS sample by BOSS. Nevertheless, the two surveys are independent, work under different seeing conditions, instrumental noise, etc., and target different types of galaxies. The correlation between the CMASS and WiggleZ data has been quantified in Ref. [79], were the authors estimated the correlation coefficient to be $\lesssim 2\%$. This justifies the inclusion of the WiggleZ data in our analysis, although their statistical weight is much lower than those from BOSS, and in practice their use does not have any important impact on our results.
(4) D_A/r_d at $z = 0.81$ measured by the Dark Energy Survey (DES)[10] [80].
(5) The anisotropic BAO data from the extended BOSS Data Release (DR) 14-quasar sample at $z = 1.19$, 1.50, 1.83 [29].
(6) The combined measurement of the anisotropic BAO information obtained from the Ly α-quasar cross- and autocorrelation of eBOSS DR14 [81,82], at $z = 2.34$.

3. Supernovae of Type Ia

We consider six effective points on the Hubble rate—i.e., $E(z) \equiv H(z)/H_0$, and the associated covariance matrix. They compress the information of 1048 SNIa contained in the Pantheon compilation [70] and the 15 SNIa at $z > 1$ from the Hubble Space Telescope Multi-Cycle Treasury programs [71]. The compression effectiveness of the information contained in such SNIa samples is extremely good, as is explicitly shown in Ref. [71]. See, e.g., Fig. 3 of that reference and the corresponding explanations in the main text.

[7] http://www.6dfgs.net/.
[8] https://www.sdss.org/.
[9] http://wigglez.swin.edu.au/site/.
[10] https://www.darkenergysurvey.org/es/.

4. Cosmic chronometers

Spectroscopic dating techniques of passively evolving galaxies—i.e., galaxies with old stellar populations and low star formation rates—have become a good tool to obtain observational values of the Hubble function at redshifts $z \lesssim 2$ [83]. These measurements do not rely on any particular cosmological model, although they are subject to other sources of systematic uncertainties, such as the ones associated with the modeling of stellar ages—see, e.g., Refs. [84,85]—which is carried out through the so-called stellar population synthesis (SPS) techniques, and also with a possible contamination due to the presence of young stellar components in such quiescent galaxies [86–88]. Given a pair of ensembles of passively evolving galaxies at two different redshifts, it is possible to infer dz/dt from observations under the assumption of a concrete SPS model and compute $H(z) = -(1+z)^{-1}dz/dt$. Thus, cosmic chronometers allow us to obtain the value of the Hubble function at different redshifts, contrary to other probes which do not directly measure $H(z)$, but integrated quantities such as, e.g., luminosity distances.

In this work, we use the 31 data points on $H(z)$ from CCH provided in Refs. [84,85,89–94]. More concretely, we make use of the *processed* sample provided in Table 2 of Ref. [95], which is more conservative, since it introduces corrections accounting for the systematic errors mentioned above.

Several authors have employed these data to reconstruct the expansion history of the Universe using Gaussian processes and/or the so-called Weighted Function Regression method [96–98]. These approaches do not rely on a particular cosmological model. They find extrapolated values of the Hubble parameter that are closer to the best-fit ΛCDM value reported by *Planck* [8], around $H_0 \sim (67.5\text{–}69.5)$ km/s/Mpc, but still compatible at $\sim 1\sigma$ C.L. with the local determination obtained with the distance ladder technique [14,99]. When BAO data and/or the SNIa from the Pantheon compilation are also incorporated in the analyses together with the CCH, the tension between the local measurement and the one inferred from the reconstruction arises again, but only at a small $\sim 2\sigma$ C.L. [96–98].

5. Redshift-space distortions

Measurements of the peculiar velocities of galaxies can be obtained from observations of their anisotropic clustering in redshift space. They allow galaxy redshift surveys to obtain constraints on the product of the growth rate of structure, $f(z) = \frac{d\ln\delta_m(a)}{d\ln a}$, and the rms of mass fluctuations at scales of $8h^{-1}$ Mpc, $\sigma_8(z)$. Much of the statistical signal comes, though, from scales where nonlinear effects and galaxy bias are significant, and they must be accurately modeled. The modeling techniques have been improved in the last few years, making data on

RSD to be a reliable tool to constrain cosmological models. These are the measurements that we include in our RSD dataset:

(1) The data point at $z = 0.03$ obtained upon combining the density and velocity fields measured by the 2MASS Tully-Fisher (2MTF) and 6dFGS peculiar velocity surveys [100].
(2) The point reported by SDSS DR7 at $z = 0.1$ [101].
(3) The two data points provided by the Galaxy and Mass Assembly survey (GAMA) at $z = 0.18$ [102] and $z = 0.38$ [103].
(4) The four points at $z = 0.22$, 0.41, 0.60, 0.78 measured by WiggleZ [104].
(5) The RSD measurements by BOSS from the power spectrum and bispectrum of the DR12 galaxies contained in the LOWZ ($z = 0.32$) and CMASS (0.57) samples [77].
(6) The two points at $z = 0.60$, 0.86 reported by the VIMOS Public Extragalactic Redshift Survey (VIPERS) [105].
(7) The point at $z = 0.77$ by the VIMOS VLT Deep Survey (VVDS) [106,107].
(8) The measurement by eBOSS DR14 at $z = 1.19$, 1.50, 1.83 [29].
(9) The Subaru FMOS galaxy redshift survey (Fast-Sound) measurement at $z = 1.36$ [108].

The internal correlations between the BAO and RSD data from Refs. [77,29] have been duly taken into account through the corresponding covariance matrices provided in these two references.

6. Prior on H_0

In some of our dataset combinations (cf. Sec. IV B), we include the prior on the Hubble parameter

$$H_{0,\mathrm{SH0ES}} = (74.03 \pm 1.42)\ \mathrm{km/s/Mpc}, \tag{8}$$

reported by the SH0ES team in Ref. [14]. It is obtained from the cosmic distance ladder and uses an improved calibration of the Cepheid period-luminosity relation, based on distances obtained from detached eclipsing binaries located in the Large Magellanic Cloud, masers in the galaxy NGC 4258, and Milky Way parallaxes. This value of the Hubble parameter is in 4.4σ tension[11] with the TTTEEE + lowE + lensing best-fit ΛCDM model of *Planck* 2018 [8], $H_0 = 67.36 \pm 0.54$ km/s/Mpc.

It has been recently argued in Ref. [109] (and later on also in Refs. [110,111]) that in cosmological studies it is better to use the SH0ES constraint on the absolute magnitude of the SNIa rather than the direct prior on H_0 when combined with low-redshift SNIa data. This is to avoid double-counting issues. We do not have this problem, though, since we do not combine the Pantheon compilation with the prior from SH0ES in any of our main analyses (cf. Sec. IV B).

7. Strong-lensing time delay distances

In combination with the prior on H_0 from SH0ES, we also use the angular diameter distances reported by the H0LICOW Collaboration.[12] They analyze six gravitationally lensed quasars of variable luminosity. After measuring the time delay between the deflected light rays and modeling the lenses, they are able to measure the so-called time-delay distances $D_{\Delta t}$ (cf. Ref. [28] and references therein). We use their reported six time-delay distances (one for each lensed system), and one distance to the deflector B1608 + 656, which according to the authors of Ref. [28] is uncorrelated with the corresponding $D_{\Delta t}$. The relevant information for building the likelihood can be found in Tables 1 and 2 of Ref. [28] and their captions. Assuming the concordance model, these distances lead to a value of $H_0 = (73.3^{+1.7}_{-1.8})$ km/s/Mpc, which is in 3.2σ tension with the one obtained from the TTTEEE + lowE + lensing analysis by *Planck* [8].

B. Combined datasets

We proceed now to describe the dataset combinations under which we have obtained the main results of this work. They are discussed in detail in Sec. V. We set constraints using the following combinations: (i) TTTEEE + lowE CMB data from *Planck* 2018 [8], in order to see the constraining power of the CMB when used alone, and also to check whether these data lead to a higher value of H_0 than in the ΛCDM. For simplicity, we will refer to this dataset as P18 throughout the paper. (ii) P18 + BSC, with BSC denoting the background dataset BAO + SNIa + CCH. (iii) We add on top of the latter the linear structure formation information contained in the RSD data, P18 + BSC + RSD. (iv) We study the impact of the CMB lensing by also adding the corresponding likelihood, P18lens + BSC + RSD. (v) Finally, we analyze the impact of the prior on H_0 from SH0ES [14] and the H0LICOW angular diameter distances [28] by using the datasets P18 + SH0ES + H0LICOW, P18lens + SH0ES + H0LICOW, and P18 + BSC + SH0ES + H0LICOW. The distance ladder and strong-lensing time delay measurements of the Hubble constant are completely independent (see, e.g., the reviews in Refs. [112,113]). When combined, they lead to

$$H_{0,\mathrm{comb}} = (73.74 \pm 1.10)\ \mathrm{km/s/Mpc}, \tag{9}$$

in 5.2σ tension with the best-fit ΛCDM value reported by *Planck* 2018 [8]. Hence, it is interesting to check what is the

[11]The tension (in terms of the number of σ) between two quantities $A \pm \sigma_A$ and $B \pm \sigma_B$ is *estimated* in this work by using the formula $|A - B|/\sqrt{\sigma_A^2 + \sigma_B^2}$, which strictly speaking is only valid if the two values are normally distributed and independent.

[12]http://shsuyu.github.io/H0LiCOW/site/.

response of the CDE model under these concrete datasets, and to compare the results with those obtained using only the CMB likelihood.

V. RESULTS

Our main results are presented in Tables I–II and Figs. 3 and 4. When we only employ the CMB temperature and polarization data from *Planck* 2018 [8] (i.e., the P18 dataset) to constrain the CDE model, the fitting values obtained for α and β are compatible at a 1σ C.L. with 0—i.e., with a cosmological constant and no interaction in the dark sector (cf. the first column in Table I). The value of H_0 remains low, roughly 4.1σ below the cosmic distance ladder measurement of Ref. [14]. Similarly, when we combine *Planck* with BSC background data or with BSC+RSD, we get values of H_0 which are 3.8σ and 3.7σ away from the SH0ES value, respectively.

As we have explained in Sec. II, there is a degeneracy between the strength of the fifth force, i.e., the parameter β, and the Hubble parameter. CDE is in principle able to lower the value of the sound horizon at the decoupling time, r_s, and the amplitude of the first peak of the $\mathcal{D}_l^{TT}$'s. The CMB data fix with high precision the angle $\theta_* = r_s/D_A^{(c)}(z_{dec})$, with $D_A^{(c)}(z_{dec})$ being the comoving angular diameter distance to the CMB last scattering surface. This means that in order to keep this ratio constant, H_0 will tend to grow for increasing values of the coupling strength, so that $D_A^{(c)}(z_{dec})$ decreases and compensates in this way the lowering of r_s, while keeping the height of the first peak compatible with data. This positive correlation between H_0 and β can be appreciated in the leftmost contour plot of Fig. 3. The latter shows 1σ and 2σ posterior probabilities for a selection of cosmological parameters. As discussed, we confirm from the first plot a mild degeneracy between H_0 and β. The strength of the fifth force does not seem to be very degenerate with σ_8, nor with the potential parameter α.

The impact of adding background data on top of P18 can be grasped by looking at the one-dimensional posterior distributions of Fig. 3 (in blue), and also at the numbers of the second column of Table I. Using the P18 + BSC combined dataset, we find that β and α are now $\sim 2.5\sigma$ and $\sim 3.1\sigma$ away from 0, respectively. The values of H_0 and σ_8, are, however, compatible at 1σ with the ones obtained using only the P18 dataset. They are also fully compatible with those obtained with the ΛCDM under the same dataset, which read $H_0 = (68.29 \pm 0.37)$ km/s/Mpc, $\sigma_8 = 0.812^{+0.006}_{-0.008}$. The peaks in β and α may indicate a mild preference of low-redshift data, when combined with the CMB, for a non-null interaction in the dark sector and a running quintessence potential. As noted already in Ref. [27], we remark that this preference does not seem to correspond to a large improvement in the minimum value of χ^2 with respect to the ΛCDM: under the P18 + BSC dataset, $\chi^2_{\rm min,CDE} - \chi^2_{\rm min,\Lambda}$ is negative, but very close to 0, which means that the CDE model is only able to improve the description of the data in a very marginal way.

The addition of the RSD data to the P18 + BSC combined dataset does not much change the result: there is a very small shift in the peak of the one-dimensional posterior distribution for α to larger values and in the one for β to lower ones (see the yellow curves in Fig. 3). These two facts reduce a little bit the value of σ_8. The aforesaid peaks are now $\sim 5\sigma$ and $\sim 2\sigma$ away from 0, respectively, with a reduction of $\chi^2_{\rm min}$ with respect to the ΛCDM of 1.56 units (cf. Table I, fourth column), i.e., pointing to a very small preference for CDE. The value of H_0 is almost unchanged.

If we include also the CMB lensing information—i.e., if we consider the P18lens + BSC + RSD combined dataset —posterior probabilities squeeze, as expected, towards the ΛCDM values. This can be seen in Fig. 4, and also in the fifth column of Table I. Given the caveats explained in Sec. IV A 1, we find it important to highlight the specific impact of CMB lensing data with respect to the P18 + BSC + RSD dataset.

In order to further evaluate the level at which the degeneracy observed in the (H_0,β) plane can alleviate the tension in the Hubble parameter between *Planck* and {SH0ES, H0LICOW} data, we perform a Monte Carlo analysis combining those data within the CDE model: results are shown in the third column in Table I and correspond to red contours in Fig. 3. In this case, the best fit corresponds to a value of $\beta = 0.0294^{+0.0120}_{-0.0076}$, i.e., at 3σ from zero coupling, a value of $\alpha = 1.32 \pm 0.18$, with $\alpha > 0$ at $\sim 7\sigma$ C.L., and $H_0 = (69.43^{+0.72}_{-0.53})$ km/s/Mpc. The raise of H_0 is possible thanks to the increase of β, which in turn needs also larger values of α. The tension with the SH0ES + H0LICOW measurement [Eq. (9)] is slightly reduced from 4.8σ (when only P18 is used to constrain the model, cf. the first column of Table I) to 3.5σ (when the SH0ES + H0LICOW data are also considered). This shifts the H_0 value 1.9σ higher than the best fit using the P18 dataset alone, within CDE. Combining also with background data, such as BSC, can partially break degeneracies and leads to $\alpha = 0.73^{+0.11}_{-0.27}$, with $\alpha > 0$ at 3.8σ and $H_0 = (68.79^{+0.35}_{-0.40})$ km/s/Mpc at 4.3σ from the SH0ES + H0LICOW value [Eq. (9)], reducing the chance of CDE to alleviate the tension, as shown in the penultimate column of the table. Finally, the impact of adding CMB lensing is shown in the last column, where now $\beta = 0.0197^{+0.0094}_{-0.0084}$ and $\alpha = 0.33^{+0.19}_{-0.23}$, with $\beta > 0$ and $\alpha > 0$ at 2.2σ and 1.6σ, respectively—i.e., shifting back towards ΛCDM. In this case $H_0 = (68.99 \pm 0.51)$ km/s/Mpc, 3.9σ away from the SH0ES + H0LICOW value [Eq. (9)], and even more had we also included BSC.

Finally, we can further quantify the relative ability of the CDE model to describe the various datasets with respect to

the ΛCDM cosmology using the Bayes ratio, in alternative to the more approximate χ^2 estimate we mentioned so far. Given a dataset $\mathcal{D}$, the probability of a certain model M_i to be the best one among a given set of models $\{M\}$ reads

$$P(M_i|\mathcal{D}) = \frac{P(M_i)\mathcal{E}(\mathcal{D}|M_i)}{P(\mathcal{D})}, \tag{10}$$

where $P(M_i)$ is the prior probability of the model M_i and $P(\mathcal{D})$ the probability of having the dataset $\mathcal{D}$. Obviously, the normalization condition $\sum_{j\in\{M\}} P(M_j) = 1$ must be fulfilled. The quantity $\mathcal{E}(\mathcal{D}|M_i)$ is the so-called marginal likelihood or evidence. If the model M_i has n parameters $p_1^{M_i}, p_2^{M_i}, \ldots, p_n^{M_i}$, the evidence takes the following form:

$$\mathcal{E}(\mathcal{D}|M_i) = \int \mathcal{L}(\mathcal{D}|\vec{p}^{M_i}, M_i)\pi(\vec{p}^{M_i})d^n p^{M_i}, \tag{11}$$

with $\mathcal{L}(\mathcal{D}|\vec{p}^{M_i}, M_i)$ being the likelihood and $\pi(\vec{p}^{M_i})$ the prior of the parameters entering the model M_i. The evidence is larger for those models that have more overlapping volume between the likelihood and the prior distributions, but it penalizes the use of additional parameters having a non-null impact on the likelihood. Hence, the evidence constitutes a good way of quantifying the performance of the model by implementing in practice the Occam razor principle. If we compare the CDE and ΛCDM models by assuming equal prior probability for both of them—i.e., $P(\text{CDE}) = P(\Lambda\text{CDM})$—then we find that the ratio of their associated probabilities is directly given by the ratio of their corresponding evidences, i.e.,

$$\frac{P(\text{CDE}|\mathcal{D})}{P(\Lambda\text{CDM}|\mathcal{D})} = \frac{\mathcal{E}(\mathcal{D}|\text{CDE})}{\mathcal{E}(\mathcal{D}|\Lambda\text{CDM})} \equiv B_{\text{CDE},\Lambda}. \tag{12}$$

This is known as the Bayes ratio and is the quantity we are interested in. For more details, we refer the reader to Refs. [17,114,115]. Notice that the computation of Eq. (12) is not an easy task in general, since we usually work with models with a high number of (mostly nuisance) parameters, so the integrals under consideration become quite involved. We have computed the evidence numerically using the Markov chains obtained from the Monte Carlo analyses and with the aid of the numerical code MCEvidence [68], which is publicly available (cf. Sec. III). We report the values obtained for the natural logarithm of the Bayes ratio [Eq. (12)] in the last row of Table I. For all the datasets under study, we find values of $\ln(B_{\text{CDE},\Lambda}) < -5$, which point to a preference of the ΛCDM over the CDE model according to Jeffreys's scale [17,114,115]. Although the CDE model we are studying here is able to reduce slightly the value of χ^2_{min} with respect to the ΛCDM, it has two additional parameters, namely α and β. Moreover, the initial value of the scalar field, ϕ_{ini}, is also left free in the Monte Carlo analysis; cf. Appendix A for details.[13] It turns out that the decrease in χ^2_{min} is insufficient to compensate the penalization introduced by the use of these extra parameters. If instead of using the evidences (11) and the Bayes ratio (12) to perform the model comparison we make use of, e.g., the Akaike [116], Bayesian [117] or Deviance [118] information criteria, we reach similar conclusions.[14] We want to note, though, that all these information criteria are approximations of the exact Bayesian approach. Although they allow us to skip the demanding computation of the evidence in Eq. (11), they are only reliable when the posterior distribution is close to a multivariate Gaussian (which is not the case under study), and the Akaike and Bayesian criteria do not take into account the impact of priors or the existing correlations between the parameters.

Similar results and conclusions are reached using an exponential potential for the scalar field, instead of Eq. (6). They are presented and discussed in Appendix C.

Finally, our results are compatible with the ones in Ref. [119]: the inclusion of background and CMB lensing shifts constraints towards ΛCDM; the model is, however, different, as ours starts from modifying the Lagrangian, which is not available in Ref. [119]. Furthermore, the source function is also different, and while the DE EOS parameter w has to be fixed to a very specific value in Ref. [119] in order to match stability conditions specific to that scenario, in our case it varies—the extra parameters lead then to a more negative Bayes ratio, preferring ΛCDM, more than claimed in Ref. [119].

VI. CONCLUSIONS

Cosmological observations help to test the dark sector, and in particular interactions between dark matter particles, mediated by a dark energy scalar field, as in CDE cosmologies. Up to a conformal transformation, this is another way of testing gravity at large scales. In this paper, we carried out this task in one of the simplest and most studied models—namely, a dark energy–dark matter conformal coupling with a Peebles-Ratra potential. CDE might probe helpful to explain the well-known tension between

[13] In the computation of the evidence [Eq. (11)] for the CDE model, we have employed the following flat priors for the extra parameters: $0 < \beta < 0.1$, $0 < \alpha < 2$, and $0 < \kappa\phi_{ini} < 50$. Slightly broader or tighter priors can be considered, but $\ln(B_{\text{CDE},\Lambda})$ only changes logarithmically, so our conclusions are not very sensitive to them.

[14] For instance, the Akaike criterion [116] is given by $\text{AIC} = \chi^2_{\text{min}} + 2n$, where n is the number of parameters in the model (the degree of correlation between them is not taken into account). Considering that CDE with PR potential has an effective number of parameters between 2 and 3, we find $2.5 < \text{AIC}_{\text{CDE}} - \text{AIC}_{\Lambda} < 6$ for the scenarios explored in Table I, which leads to a positive preference for ΛCDM, again using Jeffreys's scale [17,114,115].

local and cosmological values of H_0. Any detection of a varying dark energy potential or interaction would clearly constitute a major result, and it is therefore important to monitor the constraints that newer data impose. This is particularly true in view of earlier results that detected a nonzero value of the coupling β [26,27].

We confirm the existence of a peak in the marginalized posterior distribution for β and α, more or less evident depending on the dataset combination. While for P18 + SH0ES + H0LICOW $\beta > 0$ at 3σ and $\alpha > 0$ at nearly 7σ, the inclusion of background data reduces the evidence to $\beta > 0$ at 2.3σ and $\alpha > 0$ at nearly 3.8σ. The inclusion of CMB lensing shifts both values to be compatible with ΛCDM within 2σ. We find it important to stress that specifically CMB lensing prefers ΛCDM, and we recall in Sec. IV A 1 the caveats that would deserve further investigation in order to make this result robust also for models that depart from ΛCDM as much as CDE. In all cases, we find that, overall, the peak does not correspond to a better Bayes ratio, and ΛCDM remains the favored model when employing Bayesian model comparison, given the extra parameters introduced within the model. With regard to H_0, we find that under the P18+SH0ES+H0LICOW combined dataset, the simple coupled model with constant coupling investigated in this work leads to a value in 3.5σ tension with Eq. (9), or in 4.3σ tension when including further background data. The values of σ_8 are also similar to those found in the ΛCDM (i.e., $\sigma_8 \sim 0.80$–0.82), even when RSD data are considered together with CMB and background data. In this case, we find $\beta = 0.010^{+0.003}_{-0.009}$ and $\beta = 0.015^{+0.007}_{-0.008}$, with and without CMB lensing, respectively. For the values of the coupling strength preferred by the data, we find the typical increase of the mass of the DM particles to be $m(\phi_{ini})/m^{(0)} - 1 \lesssim \mathcal{O}(1)\%$.

The question that naturally arises is then, which modification of CDE can help in alleviating the tensions? One can immediately suppose that a varying β can go some way toward this. Or, it could be that a model with both energy and momentum couplings (see, e.g., Ref. [120]), which can introduce a weaker gravity, helps with the tensions. These issues will be investigated in future publications.

ACKNOWLEDGMENTS

We thank our institutions for allowing us to work remotely during the COVID-19 pandemic. A. G. V. is funded by the Deutsche Forschungsgemeinschaft (DFG) —Project No. 415335479.

APPENDIX A: AVOIDING THE SHOOTING

IDEA takes as input parameters the current energy densities of the various species and applies a shooting method (see, e.g., Ref. [121]) to find the initial energy densities that lead to the present-day values specified in the input. This is, of course, a very useful and convenient way of implementing the model, since very often we are interested in computing theoretical quantities by fixing the current energy densities to concrete values, most of the times very close to the best-fit ΛCDM ones. This trial and error method is unavoidable if one wants to do so. Nevertheless, this is not the most efficient way to proceed at the level of the Monte Carlo analysis. The avoidance of the shooting recursive process by directly using as input parameters the initial conditions of the energy densities instead of their current values allows us to save precious computational time. In our implementation of the CDE model in CLASS [63], we have skipped the shooting method proceeding in this way. The current energy densities and other quantities of interest, e.g., H_0 or σ_8, are obtained as derived parameters after solving the complete set of Einstein-Boltzmann equations up to $a = 1$. We also use as an input parameter in the Monte Carlo the initial value of the scalar field, $\phi_{ini} = \phi(a_{ini}) > 0$, with $a_{ini} = 10^{-14}$. On the contrary, $\phi'_{ini} = \phi'(a_{ini})$ can be expressed in terms of other input parameters. Let us show how. By solving Eq. (3) in the radiation-dominated epoch (RDE), we find

$$\phi'(\tau) = 150\beta \frac{\Omega_{dm}(a_{ini})}{\kappa a_{ini}} \varsigma \sqrt{\omega_r^*} + \frac{c_0}{\tau^2}, \tag{A1}$$

where c_0 is a dimensionless integration constant, $\varsigma \equiv 1\ \mathrm{km/s/Mpc} = 2.1332 \times 10^{-44}$ GeV (in natural units), and $\omega_r^* = \omega_\gamma(1 + 0.2271 N_{\mathrm{eff}})$ is the reduced density parameter of radiation during the RDE. We consider three massive neutrinos with equal mass and $\sum_\nu m_\nu = 0.06$ eV, so $N_{\mathrm{eff}} = 3.046$. The parameter ω_γ is determined by the temperature of the CMB photons at present, which we set to the value reported in Ref. [122], $T_\gamma^{(0)} = 2.7255$ K. Notice that the ratio $\Omega_{dm}(a)/a$ appearing in Eq. (A1) is kept constant during the RDE. To understand this, let us consider Eq. (4). It can be rewritten as

$$\rho'_{dm} + 3\mathcal{H}\rho_{dm}\left(1 - \beta\sqrt{\frac{2}{3}\Omega_{\phi,\mathrm{kin}}(a)}\right) = 0, \tag{A2}$$

with $\Omega_{\phi,\mathrm{kin}}$ being the fraction of scalar field kinetic energy in the Universe. During the RDE, $\Omega_{\phi,\mathrm{kin}} \sim 0$. In addition, $\beta \ll 1$, so we find that $\rho_{dm} \sim a^{-3}$, and hence, $\Omega_{dm}(a)/a = \mathrm{const} = \Omega_{dm}(a_{ini})/a_{ini}$. The first term on the rhs of Eq. (A1) is, therefore, constant. The solution (A1) does not depend on the form of the scalar field potential, since the impact of the latter is completely negligible during the RDE, and consists of a constant term plus a fast-decaying mode, which we will call ϕ'_{cons} and ϕ'_{dec}, respectively. In order to fulfill the BBN constraint on the total energy density at $a_{\mathrm{BBN}} \sim 10^{-9}$, one needs to demand $\rho_\phi(a_{\mathrm{BBN}}) \lesssim 0.1\rho_r(a_{\mathrm{BBN}})$ [123]. This leads to the following condition: $|c_0| < 10^{53}$. Now, using the value of c_0 that saturates the

TABLE II. Constraints for the ΛCDM, PR, CDE with flat potential and general CDE models obtained using the P18 + BSC + RSD dataset. See the comments in Appendix B.

Parameter	ΛCDM	Peebles-Ratra	CDE with $\alpha = 0$	CDE
$\Omega_{dm}^{(0)}h^2$	0.1188 ± 0.0008	$0.1180^{+0.0010}_{-0.0009}$	$0.1187^{+0.0006}_{-0.0008}$	0.1187 ± 0.0008
$\Omega_{b}^{(0)}h^2$	0.02252 ± 0.00012	0.02257 ± 0.00014	0.02253 ± 0.00011	$0.02253^{+0.00010}_{-0.00012}$
τ	$0.0508^{+0.0048}_{-0.0072}$	$0.0532^{+0.0063}_{-0.0079}$	0.0496 ± 0.0047	0.0501 ± 0.0052
H_0 [km/s/Mpc]	68.50 ± 0.34	$67.68^{+0.61}_{-0.52}$	$68.55^{+0.38}_{-0.31}$	$68.64^{+0.30}_{-0.38}$
n_s	0.9696 ± 0.0034	0.9719 ± 0.0038	$0.9700^{+0.0032}_{-0.0037}$	$0.9701^{+0.0029}_{-0.0033}$
σ_8	0.8033 ± 0.0057	$0.7880^{+0.0110}_{-0.0097}$	0.8022 ± 0.0054	0.8048 ± 0.0052
α	⋯	$0.096^{+0.038}_{-0.071}$	⋯	$0.67^{+0.11}_{-0.16}$
β	⋯	⋯	$0.0040^{+0.0012}_{-0.0032}$	$0.0151^{+0.0073}_{-0.0083}$
$\chi^2_{\mathrm{min},i} - \chi^2_{\mathrm{min},\Lambda}$	⋯	−1.74	−1.02	−1.56
$\ln B_{i,\Lambda}$	⋯	−1.67	−5.14	−8.33

upper bound, we can evaluate the ratio $\phi'_{\mathrm{dec}}(a)/\phi'_{\mathrm{cons}}(a)$ at any moment of the RDE [knowing that $a(\tau) = 100\tau\varsigma\sqrt{\omega_r^*}$]. In particular, we can compute it at a moment near the end of the RDE, e.g., at $\tilde{a} = 10^{-4}$, and see whether the decaying mode can still play an important role at that time. If we do so, we obtain $\phi'_{\mathrm{dec}}(\tilde{a})/\phi'_{\mathrm{cons}}(\tilde{a}) \approx 10^{-5}/\beta$. The values of the coupling strength explored in our Monte Carlo analyses are in the range $10^{-3} \lesssim \beta \lesssim 10^{-1}$, so we find

$$10^{-4} \lesssim \frac{\phi'_{\mathrm{dec}}(\tilde{a})}{\phi'_{\mathrm{cons}}(\tilde{a})} \lesssim 10^{-2}. \tag{A3}$$

This tells us that the decaying mode will play no role in our analysis (even when c_0 takes the largest value allowed by the BBN condition), since the observables that we use to constrain the CDE model in this work are insensitive to ϕ' at even lower values of the scale factor, i.e., at $a < \tilde{a}$. This is very positive because, in practice, this allows us to set the initial condition of $\phi'(a_{ini}) = \phi'_{\mathrm{cons}}(a_{ini})$ and reduce in this way the number of parameters that are varied in each step of the Monte Carlo. This also helps to improve the efficiency of our code.

APPENDIX B: RESULTS FOR THE NESTED MODELS

Here we present and discuss the fitting results for the two nested models of the CDE scenario that are obtained by turning off the interaction, and also by using a constant potential while keeping active the interaction in the dark sector. These two models are obtained from the general CDE scenario described in Sec. II by setting $\beta = 0$ and $\alpha = 0$, respectively. The former corresponds to the PR model [23,24]. In Table II, we show the constraints obtained for these models in the light of the P18 + BSC + RSD dataset, and also compare their statistical performance with the ΛCDM and the full CDE model. In practice, they both have one additional parameter with respect to the ΛCDM. The PR model has a very effective attractor solution for ϕ and ϕ' during the radiation-dominated epoch, which can be used to fix the initial conditions of the scalar field and its derivative, so only α enters as an additional parameter (see, e.g., Ref. [60]). On the other hand, the CDE model with flat potential only has β as extra parameter, since the equations are invariant under translations of the scalar field, and hence ϕ_{ini} can be fixed to an arbitrary value, e.g., 0. Moreover, ϕ'_{ini} can be set as explained in Appendix A. Table II shows that in the context of the PR model, it is possible to obtain much lower values of σ_8, loosening in this way the σ_8 tension. H_0, though, is below the value obtained with the ΛCDM and the other two nested models. These results are fully aligned with those from Ref. [62], but now we obtain lesser levels of evidence for the PR model, basically due to the use of the CMB high multipole polarization data, which were not employed in that reference. The reduction in the value of χ^2_{min} with respect to the ΛCDM is ∼2 units, but $\ln(B_{\mathrm{PR},\Lambda}) < -3$, so there is still more evidence for the concordance model when compared with the PR. One thing that we should explain is why the value of χ^2_{min} obtained with the PR model is lower than in the general CDE model. We would expect this not to happen, since the latter is an extension of the former, with two extra free parameters. The reason is the following: In our Monte Carlo analysis for the CDE model we cannot explore the region of parameter space with a pure PR behavior. In order for this to happen, we should produce values of β in our chains much lower than the ones we actually produce (which are in all cases greater than $\sim 10^{-3}$ due to the flat prior on $\beta > 0$ and its typical variance). These values of β always give rise to non-completely negligible effects in the MDE, and hence there is always a departure from the pure PR model. Thus, it is not strange that we find points in the parameter space of the PR model which lead to lower values of χ^2 than those found in our analysis of the CDE.

The values of the parameters obtained for the CDE model with $\alpha = 0$ remain very close to the ΛCDM ones

(cf. the third column of Table II). The model sticks to the ΛCDM because in this case there is no varying potential able to compensate the effects generated by the non-null coupling, so β is forced to remain small. In terms of Occam's razor and the corresponding Bayes ratio, there is a preference for the ΛCDM. The central value of β is almost 4 times smaller than in the general CDE model. Something similar happens in the PR model for α, which is now ∼7 times smaller than in the general CDE scenario. Due to the fact that α and β can compensate effects from each other, in the general CDE model these two parameters can be quite larger, as it is seen in the last column of Table II.

APPENDIX C: CONSTRAINTS ON CDE WITH EXPONENTIAL POTENTIAL

In this brief appendix, we complement the results provided in the main body of the paper, which have been obtained using the power-law potential [Eq. (6)]. In Table III, we provide constraints on CDE with the exponential potential

$$V(\phi) = V_0 e^{-\lambda\kappa\phi}. \tag{C1}$$

The constant $\lambda > 0$ controls its steepness. As mentioned in Sec. II, the quintessence potential only rules the scalar field dynamics in the late-time Universe, after the ϕMDE epoch, when the effects coming from the interaction in the dark sector are already subdominant. Therefore, we should not expect a change in the form of the potential to affect severely the constraints on the coupling strength β, and this is actually what we find. By comparing the results provided in Tables I and III obtained under the same datasets, we notice that both the central values and the uncertainties for β are almost identical. They are also similar to the values reported in Table II of Ref. [33], which were obtained using the CMB likelihoods from *Planck* 2015, older SNIa, BAO, and CCH data, and also older distance ladder priors on the Hubble parameter. Our constraints are a little bit tighter due to the updated (richer) datasets employed here. Also, the values of λ are quite similar. We note, though, that the central values of H_0 are mildly ($\sim 1\sigma$) lower than those obtained with the Peebles-Ratra potential. The values of $\ln B_{\mathrm{CDE},\Lambda}$ are higher (lower in absolute value), since in this model the goodness of fit is kept at the same level as in the CDE model with PR potential, and ϕ_{ini} plays no role and can be fixed, reducing thereby the complexity of the model. But they are still below −5. The results obtained with Eq. (C1) are hence fully consistent with those derived with Eq. (6).

TABLE III. Mean values and 68% C.L. uncertainties for the relevant parameters of the CDE model with exponential potential (C1), obtained with three alternative datasets. See the corresponding comments in the main text of Appendix C.

Parameter	P18 + BSC	P18 + SH0ES+ H0LICOW	P18lens + BSC+ RSD
H_0	$67.86^{+0.64}_{-0.46}$	69.29 ± 0.61	67.67 ± 0.62
σ_8	$0.8090^{+0.0110}_{-0.0090}$	0.8097 ± 0.0086	0.7994 ± 0.0084
λ	$0.40^{+0.20}_{-0.24}$	<0.163	$0.54^{+0.24}_{-0.17}$
β	$0.0198^{+0.0100}_{-0.0120}$	$0.0240^{+0.0150}_{-0.0120}$	$0.0167^{+0.0085}_{-0.0100}$
$\ln B_{\mathrm{CDE},\Lambda}$	−5.88	−6.54	−5.33

[1] A. G. Riess *et al.* (Supernova Search Team), Astron. J. **116**, 1009 (1998).
[2] S. Perlmutter *et al.* (Supernova Cosmology Project), Astrophys. J. **517**, 565 (1999).
[3] S. Cole *et al.* (2dFGRS Collaboration), Mon. Not. R. Astron. Soc. **362**, 505 (2005).
[4] D. J. Eisenstein *et al.* (SDSS Collaboration), Astrophys. J. **633**, 560 (2005).
[5] G. Hinshaw *et al.* (WMAP Collaboration), Astrophys. J. Suppl. Ser. **208**, 19 (2013).
[6] P. A. R. Ade *et al.* (Planck Collaboration), Astron. Astrophys. **571**, A1 (2014).
[7] P. A. R. Ade *et al.* (Planck Collaboration), Astron. Astrophys. **594**, A13 (2016).
[8] N. Aghanim *et al.* (Planck Collaboration), arXiv:1807.06209.
[9] S. Weinberg, Rev. Mod. Phys. **61**, 1 (1989).
[10] J. Martin, C. R. Phys. **13**, 566 (2012).
[11] J. Solà Peracaula, J. Phys. Conf. Ser. **453**, 012015 (2013).
[12] P. J. E. Peebles and B. Ratra, Rev. Mod. Phys. **75**, 559 (2003).
[13] T. Padmanabhan, Phys. Rep. **380**, 235 (2003).
[14] A. G. Riess, S. Casertano, W. Yuan, L. M. Macri, and D. Scolnic, Astrophys. J. **876**, 85 (2019).
[15] E. Macaulay, I. K. Wehus, and H. K. Eriksen, Phys. Rev. Lett. **111**, 161301 (2013).
[16] H. Hildebrandt *et al.*, Astron. Astrophys. **633**, A69 (2020).
[17] L. Amendola and S. Tsujikawa, *Dark Energy: Theory and Observations* (Cambridge University Press, Cambridge, England, 2015).
[18] A. Joyce, B. Jain, J. Khoury, and M. Trodden, Phys. Rep. **568**, 1 (2015).
[19] C. Wetterich, Astron. Astrophys. **301**, 321 (1995).
[20] L. Amendola, Phys. Rev. D **62**, 043511 (2000).
[21] R. D. Peccei, J. Solà Peracaula, and C. Wetterich, Phys. Lett. B **195**, 183 (1987).
[22] C. Wetterich, Nucl. Phys. **B302**, 668 (1988).

[23] P. J. E. Peebles and B. Ratra, Astrophys. J. **325**, L17 (1988).
[24] B. Ratra and P. J. E. Peebles, Phys. Rev. D **37**, 3406 (1988).
[25] V. Pettorino, L. Amendola, C. Baccigalupi, and C. Quercellini, Phys. Rev. D **86**, 103507 (2012).
[26] V. Pettorino, Phys. Rev. D **88**, 063519 (2013).
[27] P. A. R. Ade *et al.* (Planck Collaboration), Astron. Astrophys. **594**, A14 (2016).
[28] K. C. Wong *et al.*, arXiv:1907.04869.
[29] H. Gil-Marín *et al.*, Mon. Not. R. Astron. Soc. **477**, 1604 (2018).
[30] J.-Q. Xia, J. Cosmol. Astropart. Phys. 11 (2013) 022.
[31] A. Pourtsidou and T. Tram, Phys. Rev. D **94**, 043518 (2016).
[32] C. van de Bruck, J. Mifsud, and J. Morrice, Phys. Rev. D **95**, 043513 (2017).
[33] C. van de Bruck and J. Mifsud, Phys. Rev. D **97**, 023506 (2018).
[34] Y.-H. Li, J.-F. Zhang, and X. Zhang, Phys. Rev. D **90**, 123007 (2014).
[35] Y.-H. Li, J.-F. Zhang, and X. Zhang, Phys. Rev. D **93**, 023002 (2016).
[36] E. Di Valentino, A. Melchiorri, and O. Mena, Phys. Rev. D **96**, 043503 (2017).
[37] E. G. M. Ferreira, J. Quintin, A. A. Costa, E. Abdalla, and B. Wang, Phys. Rev. D **95**, 043520 (2017).
[38] A. A. Costa, X.-D. Xu, B. Wang, and E. Abdalla, J. Cosmol. Astropart. Phys. 01 (2017) 028.
[39] J. Solà Peracaula, A. Gómez-Valent, and J. de Cruz Pérez, Phys. Lett. B **774**, 317 (2017).
[40] J. Solà Peracaula, J. de Cruz Pérez, and A. Gómez-Valent, Mon. Not. R. Astron. Soc. **478**, 4357 (2018).
[41] M. Martinelli, N. B. Hogg, S. Peirone, M. Bruni, and D. Wands, Mon. Not. R. Astron. Soc. **488**, 3423 (2019).
[42] P. Agrawal, G. Obied, and C. Vafa, arXiv:1906.08261.
[43] S. Pan, G. S. Sharov, and W. Yang, Phys. Rev. D **101**, 103533 (2020).
[44] J. Solà Peracaula, J. de Cruz Pérez, and A. Gómez-Valent, Europhys. Lett. **121**, 39001 (2018).
[45] A. Gómez-Valent and J. Solà Peracaula, Mon. Not. R. Astron. Soc. **478**, 126 (2018).
[46] P. Tsiapi and S. Basilakos, Mon. Not. R. Astron. Soc. **485**, 2505 (2019).
[47] L. Amendola, Phys. Rev. D **69**, 103524 (2004).
[48] V. Pettorino and C. Baccigalupi, Phys. Rev. D **77**, 103003 (2008).
[49] L. Amendola and V. Pettorino, Phys. Lett. B **802**, 135214 (2020).
[50] C. M. Will, Living Rev. Relativity **9**, 3 (2006).
[51] B. Elder, V. Vardanyan, Y. Akrami, P. Brax, A.-C. Davis, and R. S. Decca, Phys. Rev. D **101**, 064065 (2020).
[52] P. Brax, A.-C. Davis, B. Elder, and L. K. Wong, Phys. Rev. D **97**, 084050 (2018).
[53] J. Bergé, P. Brax, G. Métris, M. Pernot-Borràs, P. Touboul, and J.-P. Uzan, Phys. Rev. Lett. **120**, 141101 (2018).
[54] G. Efstathiou and S. Gratton, arXiv:2002.06892.
[55] R. K. Sachs and A. M. Wolfe, Astrophys. J. **147**, 73 (1967); Gen. Relativ. Gravit. **39**, 1929 (2007).
[56] L. Amendola, V. Pettorino, C. Quercellini, and A. Vollmer, Phys. Rev. D **85**, 103008 (2012).
[57] M. Baldi, V. Pettorino, G. Robbers, and V. Springel, Mon. Not. R. Astron. Soc. **403**, 1684 (2010).
[58] M. Baldi and V. Pettorino, Mon. Not. R. Astron. Soc. **412**, L1 (2011).
[59] L. Amendola and C. Quercellini, Phys. Rev. D **68**, 023514 (2003).
[60] J. Solà Peracaula, A. Gómez-Valent, and J. de Cruz Pérez, Mod. Phys. Lett. A **32**, 1750054 (2017).
[61] J. Ooba, B. Ratra, and N. Sugiyama, Astrophys. Space Sci. **364**, 176 (2019).
[62] Joan Solà Peracaula, A. Gómez-Valent, and J. de Cruz Pérez, Phys. Dark Universe **25**, 100311 (2019).
[63] D. Blas, J. Lesgourgues, and T. Tram, J. Cosmol. Astropart. Phys. 07 (2011) 034.
[64] V. Pettorino, L. Amendola, and C. Wetterich, Phys. Rev. D **87**, 083009 (2013).
[65] L. Amendola, M. Baldi, and C. Wetterich, Phys. Rev. D **78**, 023015 (2008).
[66] B. Audren, J. Lesgourgues, K. Benabed, and S. Prunet, J. Cosmol. Astropart. Phys. 02 (2013) 001.
[67] A. Lewis, arXiv:1910.13970.
[68] A. Heavens, Y. Fantaye, A. Mootoovaloo, H. Eggers, Z. Hosenie, S. Kroon, and E. Sellentin, arXiv:1704.03472.
[69] M. Betoule *et al.* (SDSS Collaboration), Astron. Astrophys. **568**, A22 (2014).
[70] D. M. Scolnic *et al.*, Astrophys. J. **859**, 101 (2018).
[71] A. G. Riess *et al.*, Astrophys. J. **853**, 126 (2018).
[72] G. Efstathiou, Mon. Not. R. Astron. Soc. **440**, 1138 (2014).
[73] N. Aghanim *et al.* (Planck Collaboration), arXiv:1807.06210.
[74] P. Carter, F. Beutler, W. J. Percival, C. Blake, J. Koda, and A. J. Ross, Mon. Not. R. Astron. Soc. **481**, 2371 (2018).
[75] F. Beutler, C. Blake, M. Colless, D. H. Jones, L. Staveley-Smith, L. Campbell, Q. Parker, W. Saunders, and F. Watson, Mon. Not. R. Astron. Soc. **416**, 3017 (2011).
[76] A. J. Ross, L. Samushia, C. Howlett, W. J. Percival, A. Burden, and M. Manera, Mon. Not. R. Astron. Soc. **449**, 835 (2015).
[77] H. Gil-Marín, W. J. Percival, L. Verde, J. R. Brownstein, C.-H. Chuang, F.-S. Kitaura, S. A. Rodríguez-Torres, and M. D. Olmstead, Mon. Not. R. Astron. Soc. **465**, 1757 (2017).
[78] E. A. Kazin *et al.*, Mon. Not. R. Astron. Soc. **441**, 3524 (2014).
[79] F. Beutler, C. Blake, J. Koda, F. Marin, H.-J. Seo, A. J. Cuesta, and D. P. Schneider, Mon. Not. R. Astron. Soc. **455**, 3230 (2016).
[80] T. M. C. Abbott *et al.* (DES Collaboration), Mon. Not. R. Astron. Soc. **483**, 4866 (2019).
[81] M. Blomqvist *et al.*, Astron. Astrophys. **629**, A86 (2019).
[82] V. de Sainte Agathe *et al.*, Astron. Astrophys. **629**, A85 (2019).
[83] R. Jiménez and A. Loeb, Astrophys. J. **573**, 37 (2002).
[84] M. Moresco *et al.*, J. Cosmol. Astropart. Phys. 08 (2012) 006.
[85] M. Moresco, L. Pozzetti, A. Cimatti, R. Jiménez, C. Maraston, L. Verde, D. Thomas, A. Citro, R. Tojeiro, and D. Wilkinson, J. Cosmol. Astropart. Phys. 05 (2016) 014.

[86] M. López-Corredoira, A. Vazdekis, C. M. Gutiérrez, and N. Castro-Rodriguez, Astron. Astrophys. **600**, A91 (2017).
[87] M. López-Corredoira and A. Vazdekis, Astron. Astrophys. **614**, A127 (2018).
[88] M. Moresco, R. Jiménez, L. Verde, L. Pozzetti, A. Cimatti, and A. Citro, Astrophys. J. **868**, 84 (2018).
[89] R. Jiménez, L. Verde, T. Treu, and D. Stern, Astrophys. J. **593**, 622 (2003).
[90] J. Simon, L. Verde, and R. Jiménez, Phys. Rev. D **71**, 123001 (2005).
[91] D. Stern, R. Jiménez, L. Verde, M. Kamionkowski, and S. A. Stanford, J. Cosmol. Astropart. Phys. 02 (2010) 008.
[92] C. Zhang, H. Zhang, S. Yuan, T.-J. Zhang, and Y.-C. Sun, Res. Astron. Astrophys. **14**, 1221 (2014).
[93] M. Moresco, Mon. Not. R. Astron. Soc. **450**, L16 (2015).
[94] A. L. Ratsimbazafy, S. I. Loubser, S. M. Crawford, C. M. Cress, B. A. Bassett, R. C. Nichol, and P. Väisänen, Mon. Not. R. Astron. Soc. **467**, 3239 (2017).
[95] A. Gómez-Valent, J. Cosmol. Astropart. Phys. 05 (2019) 026.
[96] H. Yu, B. Ratra, and F.-Y. Wang, Astrophys. J. **856**, 3 (2018).
[97] A. Gómez-Valent and L. Amendola, J. Cosmol. Astropart. Phys. 04 (2018) 051.
[98] B. S. Haridasu, V. V. Lukovi, M. Moresco, and N. Vittorio, J. Cosmol. Astropart. Phys. 10 (2018) 015.
[99] A. G. Riess *et al.*, Astrophys. J. **855**, 136 (2018).
[100] F. Qin, C. Howlett, and L. Staveley-Smith, Mon. Not. R. Astron. Soc. **487**, 5235 (2019).
[101] F. Shi *et al.*, Astrophys. J. **861**, 137 (2018).
[102] F. Simpson, C. Blake, J. A. Peacock, I. Baldry, J. Bland-Hawthorn, A. Heavens, C. Heymans, J. Loveday, and P. Norberg, Phys. Rev. D **93**, 023525 (2016).
[103] C. Blake *et al.*, Mon. Not. R. Astron. Soc. **436**, 3089 (2013).
[104] C. Blake *et al.*, Mon. Not. R. Astron. Soc. **415**, 2876 (2011).
[105] F. G. Mohammad *et al.*, Astron. Astrophys. **619**, A17 (2018).
[106] L. Guzzo *et al.*, Nature (London) **451**, 541 (2008).
[107] Y.-S. Song and W. J. Percival, J. Cosmol. Astropart. Phys. 10 (2009) 004.
[108] T. Okumura *et al.*, Publ. Astron. Soc. Jpn. **68**, 38 (2016).
[109] D. Camarena and V. Marra, Mon. Not. R. Astron. Soc. **495**, 2630 (2020).
[110] S. Dhawan, D. Brout, D. Scolnic, A. Goobar, A. G. Riess, and V. Miranda, Astrophys. J. **894**, 54 (2020).
[111] G. Benevento, W. Hu, and M. Raveri, Phys. Rev. D **101**, 103517 (2020).
[112] L. Verde, T. Treu, and A. G. Riess, Nat. Astron. **3**, 891 (2019).
[113] A. G. Riess, Nat. Rev. Phys. **2**, 10 (2020).
[114] R. E. Kass and A. E. Raftery, J. Am. Stat. Assoc. **90**, 773 (1995).
[115] K. P. Burnham and D. R. Anderson, *Model Selection and Multimodel Inference* (Springer, New York, 2002).
[116] H. Akaike, IEEE Trans. Autom. Control **19**, 716 (1974).
[117] G. Schwarz, Ann. Stat. **6**, 461 (1978).
[118] D. J. Spiegelhalter, N. G. Best, B. P. Carlin, and A. van der Linde, J. R. Stat. Soc. **64**, 583 (2002).
[119] E. Di Valentino, A. Melchiorri, O. Mena, and S. Vagnozzi, Phys. Rev. D **101**, 063502 (2020).
[120] L. Amendola and S. Tsujikawa, arXiv:2003.02686.
[121] J. Stoer and R. Bulirsch, *Introduction to Numerical Analysis* (Springer-Verlag, New York, 1980).
[122] D. J. Fixsen, Astrophys. J. **707**, 916 (2009).
[123] J.-P. Uzan, Living Rev. Relativity **14**, 2 (2011).